# Shape-memory-assisted self-healing of macroscopic punctures from periodic dynamic polymers with high energy density and tunable actuation temperature

Yuran Shi<sup>1,2†</sup>, Christopher B. Cooper<sup>2†</sup>, Tomoko Nogusa<sup>2,3</sup>, Jian-Cheng Lai<sup>2</sup>, Hao Lyu<sup>2</sup>, Muhammad Khatib<sup>2</sup>, Chengyi Xu<sup>2</sup>, Lukas Michalek<sup>2</sup>, Zhenan Bao<sup>2\*</sup>.

<sup>&</sup>lt;sup>1</sup>Department of Chemistry, Stanford University, Stanford, CA 94305

<sup>&</sup>lt;sup>2</sup>Department of Chemical Engineering, Stanford University, Stanford, CA 94305

<sup>&</sup>lt;sup>3</sup>Corporate Research and Development, Research Laboratory of Advanced Science & Technology, Asahi Kasei Corporation, Fuji, Japan

<sup>†</sup>Equal contribution

<sup>\*</sup>Corresponding author. Email: <u>zbao@stanford.edu</u>

### **ABSTRACT**

Shape memory polymers (SMPs) have potential applications in areas such as wearable electronics, implantable biomedical devices, and soft robotics. However, most SMPs suffer from low energy densities, which limits the maximum load that can be sustained during actuation. Recent work has shown that periodically incorporating directional hydrogen bonds can enable high energy density SMPs by forming stable strain-induced supramolecular nanostructures. In this work, we show that modifying the polymer molecular design by incorporating additional weaker H-bonding units allows tuning of the SMP actuation temperature (from 60 to 25 °C) while maintaining almost 80% of the energy density of the original polymer. Moreover, these modifications enable self-healing at accessible temperatures (~70 °C). By combining high energy density shape memory behavior with self-healing properties, we realized rapid healing of large (i.e., centimeter scale), macroscopic damages (e.g., knife punctures), which were unable to heal in similar polymers without high energy density or the shape-memory-assisted self-healing (SMASH) behavior. As a comparison, previously reported lower energy density SMPs only showed healing of submillimeter-sized scratches or punctures. The self-healing SMP was used to fabricate a force sensor that exhibited self-healing ability, high cyclability, and high sensitivity. Our work demonstrates that the incorporation of periodic dynamic bonds and the resulting formation of strain-induced supramolecular structures are promising mechanisms for the design of tunable, high energy density shape memory polymers for applications in smart, self-healing wearable devices with superior performance and durability.

### INTRODUCTION

Shape memory polymers (SMP), which can readily switch from a temporary shape to a permanent shape when exposed to external stimuli, are promising materials for emerging applications such as wearable electronics, smart biomedical devices, soft robotics, and space-deployable structures.<sup>[1–5]</sup> In addition, SMPs have the potential to replace alternatives such as shape memory alloys due to their low production cost, light weight, processability, and high shape recovery.<sup>[6–9]</sup> However, many reported SMPs face challenges including low energy density, limited toughness, and insufficient recovery stress.<sup>[8,10]</sup>

Cooper et. al have reported an SMP design to overcome the above drawbacks by periodically incorporating strong H-bonding units into the polymer backbone to form strain-induced long-range order of supramolecular nanostructures. [4,11] Since then, Liu and his coworkers have developed other high energy density SMPs incorporating this strategy, but they all have high glass transition temperatures  $(T_g)$ . [12,13] Since actuation is initiated when the supramolecular nanostructures are disrupted above  $T_g$  [4], this results in high actuation temperatures and prevents actuation at physiologically safe temperatures (near 37 °C). Moreover, increasing the polymer  $T_g$  limits the self-healability of the SMPs [14,15], which is undesirable for two reasons. First, making SMPs self-healable can improve their durability in wearable electronic and soft robotic applications. [16-21] Second, previous reports have shown that shape memory behavior can aid in self-healing, by enabling automatic and rapid closure, but these reports have been limited to low energy density materials and minor damages such as scratches and indentation. [15,18,22-26]

In this work, we design a set of shape memory polymers, abbreviated as PPG-MPU<sub>x</sub>-PA<sub>1-x</sub>, (**Figure 1A**) with varying ratios of strong (MPU, 4,4'-methylenebisphenyl urea)<sup>[27–29]</sup> and weak (PA, p-phenylenediamide) dynamic bonds<sup>[30]</sup> to tune  $T_g$  (from -7 to 39 °C) and polymer dynamics. These SMPs have tunable actuation temperatures and self-healing capabilities, while also maintaining high energy density. We observe a strong relationship between actuation temperature and  $T_g$  in the PPG-MPU<sub>x</sub>-PA<sub>1-x</sub> polymers, suggesting control of  $T_g$  as a key molecular design parameter for the development of high energy density in these SMPs.

Moreover, we hypothesized that the combination of high energy density shape memory behavior and accessible terminal flow temperatures would enable rapid self-healing from large-area puncture damages, which was only possible previously with capsule and vascular based self-healing mechanisms.<sup>[31,32]</sup>

Normally, the self-healing rate of polymers, based on reversible dynamic bonds, is limited by the rate of bulk chain diffusion or open sticker diffusion and thus require a longer healing time for larger damages,

and in some cases never recover. [33,34] While Cooper et al. recently have shown the methods for the potential of multiple layers realignment during self-healing, these methods fail for larger damages when layers are not in initial contact. [35] Furthermore, Rodriguez et al. showed combining shape memory behavior with conventional self-healing abilities (i.e., shape-memory-assisted self-healing, SMASH<sup>[15]</sup>) facilitated the closure of small scratch and nanoindentation.<sup>[16,36,37]</sup> However, the extent of self-healing was limited to minor scratches, primarily because the low energy density of the SMP means that it is unable to actuate large fractured pieces, preventing the closure of the macroscopic wounds. Here, we show using high-energy density and excellent shape recovery SMP enable the polymer to quickly return to its original shape by the shape memory effect after large damage (centimeter size), followed by subsequent annealing to repair cracked interfaces. The best performing polymer, that exhibited shapememory effects near room-temperature and fastest healing rate, PPG-MPU<sub>0.7</sub>-PA<sub>0.3</sub>, can fully self-heal from a puncture that is 40 mm in length and 6 mm in width created by a twisting blade as well as a 1 cm by 1 cm puncture created by a screwdriver after healing for 36 hours at 70 °C. The high energy density SMP enables the deformed creases near the puncture to pull the fractured pieces back to the original location and make contact. Conversely, a similar polymer, PPG-MPU<sub>0.5</sub>-PA<sub>0.5</sub>, which exhibits faster traditional self-healing but lacks shape memory behavior at room temperature, is unable to heal from the same large damage, even with long healing times. Finally, we use PPG-MPU<sub>0.7</sub>-PA<sub>0.3</sub> to design a selfhealing pressure sensor to show the potential for these materials in wearable electronics and smart biomedical devices.

#### RESULTS

Our previous work has shown that the formation of strain-induced supramolecular structures can be used to achieve one-way shape memory polymers with high energy density, using polypropylene glycol (PPG) and 4,4'-methylene biphenylurea (MPU).<sup>[4]</sup> Here we modify the PPG-MPU structure by incorporating *p*-phenylenediamide (PA) units along the backbone in place of MPU at varying molar fractions (**Figure 1A**). We found that tuning their ratios allowed us to optimize the shape memory actuation temperature and self-healing properties to enable shape-memory assisted self-healing (SMASH), which allows polymer films to rapidly and autonomously recover from large puncture damages (**Figure 1B**).

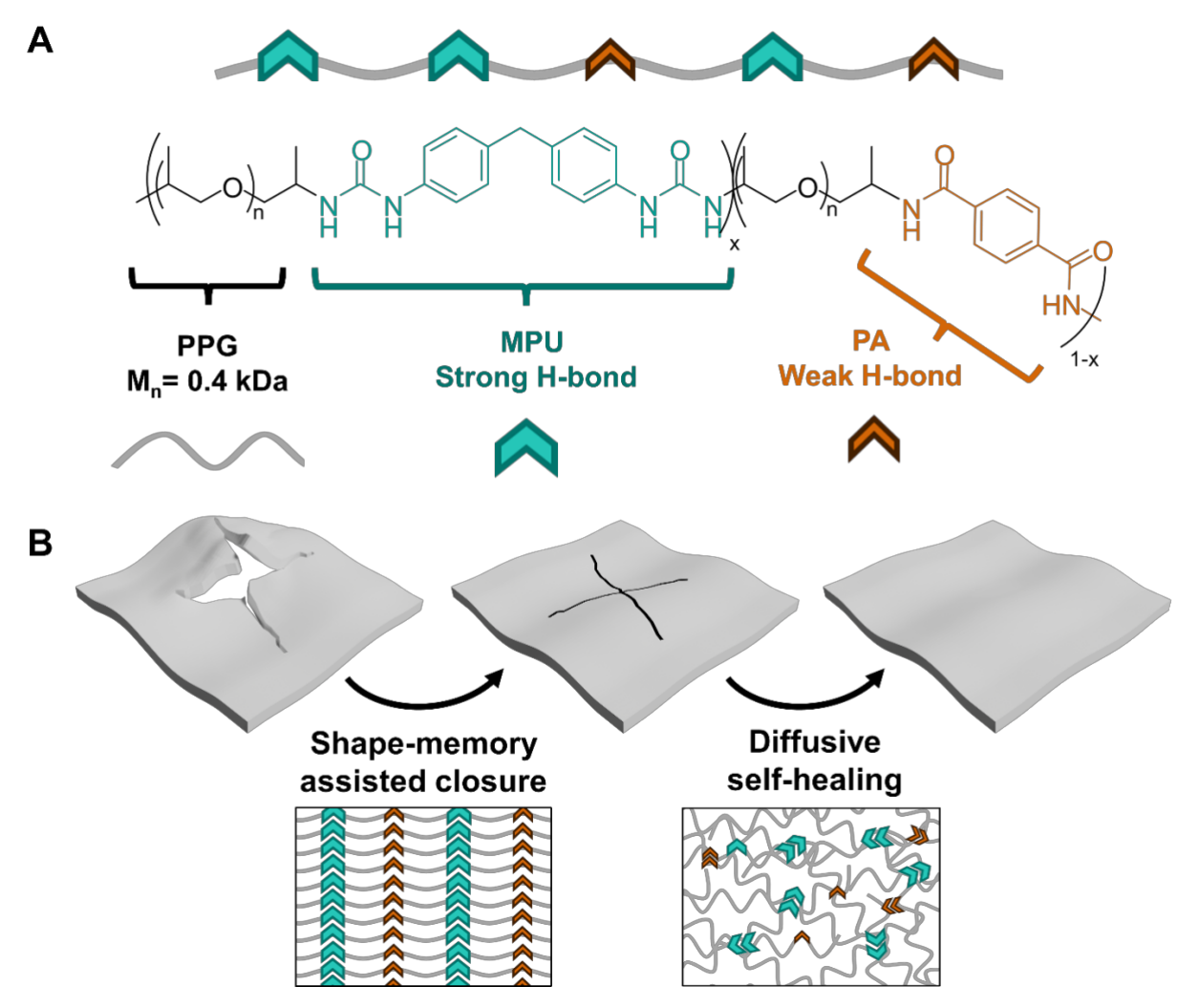


**Figure 1. Molecular design of PPG-MPU**<sub>x</sub>-**PA**<sub>1-x</sub> **polymers. A)** Schematic and chemical structure of the PPG-MPU<sub>x</sub>-PA<sub>1-x</sub> polymers. They combine strong H-bonding MPUs (4,4'-methylenebisphenyl urea) with weak H-bonding PAs (*p*-phenylenediamide) along a polypropylene glycol (PPG) backbone. **B)** Schematic of shape-memory assisted self-healing (SMASH) mechanism in periodic dynamic polymers. After damage, high energy density shape memory behavior, enabled by the formation of strain-induced supramolecular structures, facilitates rapid closure of the damaged areas back into contact. Subsequent annealing of the polymer film enables traditional, diffusive self-healing to repair interfacial cracks for full recovery of the polymer film.

We synthesized a set of seven polymers with varying MPU:PA molar ratios as indicated in **Table 1** and verified successful polymerization by  ${}^{1}$ H nuclear magnetic resonance (NMR) and gel permeation chromatography (GPC) (**Table 1, Figure S1-9**). Differential scanning calorimetry (DSC) traces of the polymers showed a clear and non-linear increase in the glass transition temperature ( $T_q$ ) with increasing

molar fraction of MPU (**Figure 2A**, **Table 1**). The  $T_g$  trend partially follows that predicted by the empirical Fox equation for amorphous blends and random copolymers, given by:

$$\frac{1}{T_{g,x}} = \frac{x_{MPU}}{T_{g,x=1}} + \frac{1 - x_{MPU}}{T_{g,x=0}} \tag{1}$$

where  $T_{g,x=1}$  is the  $T_g$  of PPG-MPU<sub>1.0</sub>,  $T_{g,x=0}$  is the  $T_g$  of PPG-PA<sub>1.0</sub> and  $T_{g,x}$  is the predicted  $T_g$  of a PPG-MPU<sub>x</sub>-PA<sub>1.x</sub> polymer (**Figure 2B**). We also performed Fourier-transform infrared spectroscopy measurements (FTIR) on the PPG-MPU<sub>x</sub>-PA<sub>1.x</sub> polymers, which show the transition from urea-dominated to amide-dominated C=O and N-H stretches from  $x_{MPU}=1$  to  $x_{MPU}=0$  (**Figure 2C-D**). [38,39] Above  $x_{MPU}=0.3$ , the PPG-MPU<sub>x</sub>-PA<sub>1.x</sub> polymers exhibited robust mechanical properties, including high stretchability, tensile strength, and toughness. (**Figure 2E-F, Table 1, Figure S10**). The polymers exhibited strain hardening between 200-300% strain and stress whitening into an opaque film above ~500% strain (**Figure 2G**). In addition, the films often fractured into tendrils instead of necking to a clean break (**Figure 2H**) and exhibited notch insensitivity (**Figure S10**). All of these observations are consistent with the formation of strain-induced supramolecular structures reported previously. [4] Moreover, from 2D x-ray diffraction (XRD) data, we observed that all of the strained  $x_{MPU}=1$ , 0.9, and 0.7 films showed increased intensity of urea-urea H-bond stacking peak perpendicular to the strain direction compared to parallel to the strain (**Figure S11**). This suggests that the polymer backbones align parallel to the strain while the urea groups stack into supramolecular nanostructures oriented perpendicular to the strain.

Table 1. Characterization of PPG-MPU<sub>x</sub>-PA<sub>1-x</sub> polymers.

Sample Name	<i>Х</i> мри	xmpu (NMR)	M <sub>n</sub> (kDa)	Ð	Glass Transition Temp., $T_g$ (°C)	Crossover Temp., $T_{xc}$ (°C)	Tensile Strength, σ (MPa)	Toughness, $U_T$ (MPa)	Actuation Temp.,  Tact (°C)	Measured Energy Density, (MJ/m³)
PPG-PA <sub>1.0</sub>	0	0	8	1.4	-7	25	-	-	-	-
PPG-MPU <sub>0.1</sub> -PA <sub>0.9</sub>	0.1	0.10	13	1.4	0	25	-	-	-	-
PPG-MPU <sub>0.3</sub> -PA <sub>0.7</sub>	0.3	0.32	11	1.5	1	49	-	-	-	-
PPG-MPU <sub>0.5</sub> -PA <sub>0.5</sub>	0.5	0.53	9	1.5	7	65	15 ± 2	$162 \pm 22$	-	-
PPG-MPU <sub>0.7</sub> -PA <sub>0.3</sub>	0.7	0.72	14	1.5	15	80	20 ± 1	232 ± 58	25-35	2.5
PPG-MPU <sub>0.9</sub> -PA <sub>0.1</sub>	0.9	0.92	11	1.4	25	105	31 ± 1	456 ± 20	35-45	2.4

PPG-MPU <sub>1.0</sub>	1.0	1.0	10	1.1	40	145	48 ± 13	872 ± 81	50-60	3.2

<sup>-</sup> The test wasn't conducted due to low  $T_g$ .

 $T_{act}$  was defined as the temperature at the half point of the actuation process; equations included in the key parameters below.

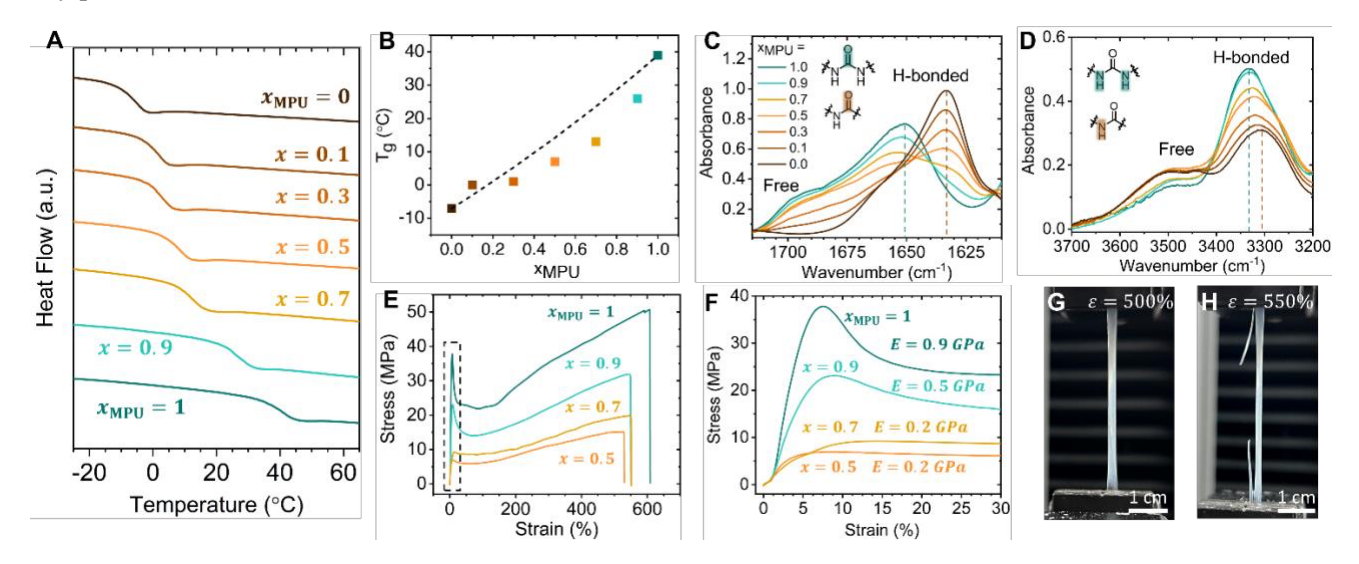


Figure 2. Thermal and mechanical properties of PPG-MPU<sub>x</sub>-PA<sub>1-x</sub> polymers. A) DSC traces  $x_{\text{MPU}} = 0$  (brown, top),  $x_{\text{MPU}} = 0.1$  (dark orange),  $x_{\text{MPU}} = 0.3$  (orange),  $x_{\text{MPU}} = 0.5$  (light orange),  $x_{\text{MPU}} = 0.7$  (yellow),  $x_{\text{MPU}} = 0.9$  (teal), and  $x_{\text{MPU}} = 1.0$  (dark teal, bottom). B) Glass transition temperatures ( $T_g$ ) extracted from the DSC data as a function of MPU mol fraction. The black dashed line shows the predicted values using the empirical Fox equation. C-D) FTIR spectrum of the urea and amide region for PPG-MPU<sub>x</sub>-PA<sub>1-x</sub> polymers. (E) Stress-strain curves (F)and zoomed low strain region for  $x_{\text{MPU}} = 0.5$ , 0.7, 0.9, and 1.0. G) Image of PPG-MPU<sub>0.7</sub>-PA<sub>0.3</sub> whitening at 500% tensile strain. H) Image of fracture behavior of PPG-MPU<sub>0.7</sub>-PA<sub>0.3</sub> during tensile testing (~550% strain).

We next characterized the rheological properties of the PPG-MPU<sub>x</sub>-PA<sub>1-x</sub> polymers under oscillatory strain (1 rad/s) between 25-145 °C (**Figure 3A**). Both PPG-PA<sub>1.0</sub> and PPG-MPU<sub>0.1</sub>-PA<sub>0.9</sub> behave as viscoelastic liquids at room temperature, consistent with their lower  $T_g$  values of -7 °C and 0 °C, respectively. Increasing the mol fraction of MPU leads to a clear increase in glassy behavior at lower temperatures, with PPG-MPU<sub>0.7</sub>-PA<sub>0.3</sub>, PPG-MPU<sub>0.9</sub>-PA<sub>0.1</sub>, and PPG-MPU<sub>1.0</sub> exhibiting a glassy plateau (G' ~ 10<sup>9</sup> Pa) in the storage modulus (G') at room temperature. Plotting the storage modulus versus temperature shifted by  $T_g$  (**Table 1**) shows that the end of the glassy plateau occurs earlier in PPG-MPU<sub>1.0</sub> relative to  $T_g$  (**Figure 3B**). All polymers showed a crossover (G' = G") into terminal flow at sufficiently high temperatures ( $T_{xc}$ ), indicating the potential for diffusive self-healing enabled by the diffusion and

recovery of open dynamic bonds and individual chains across the damaged interface. Previous experimental work has shown that this terminal flow temperature ( $T_{xc}$ ) is roughly equivalent to the self-healing temperature, which is the lowest temperature required for the polymer to be self-healed measured on rheometer.<sup>[35]</sup>.  $T_{xc}$  increased with increasing  $x_{MPU}$  (**Figure 3C**), with PPG-MPU<sub>1.0</sub> showed the highest  $T_{xc}$  of 145 °C, and consequently the slowest self-healing at room temperature or elevated temperature. By decreasing the  $x_{MPU}$  to 0.9,  $T_{xc}$  decreased to 105 °C and decreasing  $x_{MPU}$  to 0.7 further lowered  $T_{xc}$  to 80 °C, which enables more accessible self-healing conditions as demonstrated later in the paper.

We next characterized the microstructures of the hot-pressed PPG-MPU<sub>x</sub>-PA<sub>1-x</sub> films by small-angle x-ray scattering (SAXS) and atomic force microscopy (AFM). SAXS scattering data for each polymer was fitted using a broad peak model commonly used for empirical determination of characteristic length scales in hydrogels or dynamic polymers with clustered domains, <sup>[40]</sup> given by:

$$I(q) = \frac{I_0}{1 + ((q - q_0)\xi_0)^2} + \frac{I_1}{1 + ((q - q_1)\xi_1)^2} + \frac{I_2}{q^N} + I_3$$
 (2)

where the first two terms are the first and second broad peaks (at different q-regimes) and the last two terms are the background scattering (**Figure S12**, **Table S1**). The parameters  $q_0$  and  $q_1$  provide the average interdomain spacing between clusters in each peak while the correlation lengths,  $\xi_0$  and  $\xi_1$ , describe the extent of interdomain positional correlations, or equivalently, the variance in interdomain spacings for each peak (i.e., full width at half maximum,  $FWHM = \frac{2}{\xi}$ ).

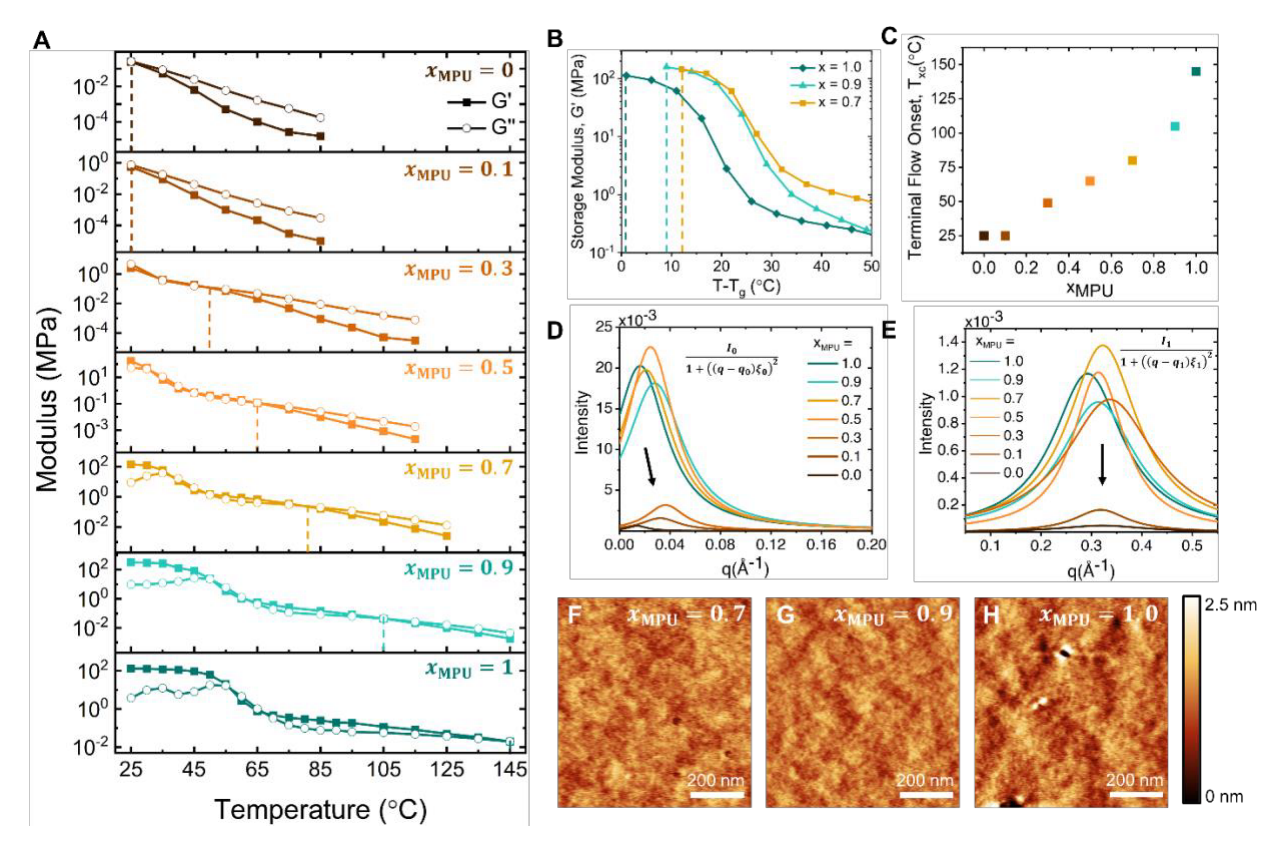


Figure 3. Rheological and microstructural characterization of PPG-MPU<sub>x</sub>-PA<sub>1-x</sub> polymers. A)

Temperature sweeps of the storage (G', solid symbols) and loss (G", open symbols) moduli for PPG-MPU<sub>x</sub>-PA<sub>1-x</sub> polymers measured at 1 rad/s. Vertical dashed lines mark the terminal flow onset temperature ( $T_{xc}$ ). **B)** Storage modulus plotted versus temperature shifted by  $T_g$  for  $x_{MPU} = 0.7$ , 0.9, and 1.0. Vertical dashed lines mark where the glassy plateau ends. **C)** Terminal flow onset temperatures for different  $x_{MPU}$  fractions extracted from the temperature sweeps. Lorentz-fitted low-q (large domain) regime peaks **D)** and high-q (small domain) regime peaks **E)** for PPG-MPU<sub>x</sub>-PA<sub>1-x</sub> polymers. AFM height images for **F)**  $x_{MPU} = 0.7$  (root-mean square roughness,  $R_q = 0.23$  nm), **G)** 0.9 ( $R_q = 0.21$  nm), and **H)** 1.0 ( $R_q = 0.32$  nm), showing amorphous morphologies with a slightly increasing roughness.

The fitted SAXS data for the polymers exhibited two broad peaks at low and high q, corresponding to large ( $q_0 \approx 0.03 \text{ Å}^{-1}$ ,  $\approx 20 \text{ nm}$ ) and small ( $q_1 \approx 0.32 \text{ Å}^{-1}$ ,  $\approx 2 \text{ nm}$ ) domain sizes, respectively (**Figure 3D-E**). For  $x_{MPU}$  above 0.5, these peaks were relatively similar. However, PPG-MPU<sub>0.3</sub>-PA<sub>0.7</sub> showed decreased large-domain aggregation, while both PPG-MPU<sub>0.1</sub>-PA<sub>0.9</sub> and PPG-PA<sub>1.0</sub> showed almost no aggregation at either length scale. Consistent with the SAXS data, AFM images of PPG-MPU<sub>0.7</sub>-PA<sub>0.3</sub>, PPG-MPU<sub>0.9</sub>-PA<sub>0.1</sub>, and PPG-MPU<sub>1.0</sub>, were almost featureless with a slight increase in roughness with increasing  $x_{MPU}$  (**Figure 3F-H**). Polymers with lower fractions of MPU were slightly sticky and could not be measured by AFM.

We next measured the shape memory properties of our polymers based on the following key parameters (**Figure 4A**):

•  $l_0$ : initial length of the polymer

•  $l_{fix}$ : fixed length of the polymer after stretching and releasing

•  $l_{final}$ : final length after heating

•  $T_{prog}$ : programming temperature during initial straining

•  $T_{act}$ : actuation temperature defined when  $l(T_{act}) = \frac{l_{fix} + l_{final}}{2}$ 

•  $\sigma_{act}$ : actuation load

•  $\sigma_{r,max}$ : recovery stress (i.e.,  $\sigma_{act}$  where  $\varepsilon_{act} = 0$ )

•  $\varepsilon_{r,max}$ : recovery strain (i.e., the maximum contraction when  $\sigma_{act}=0$ )

•  $\varepsilon_{act}$ : contraction strain achieved during actuation defined as  $\frac{l_{fix} - l_{final}}{l_{fix}}$ 

We tested the samples by straining the polymers to 300%, releasing them, and then heating under a fixed actuation load  $\sigma_{act}$  to extract values of  $l_{fix}$ ,  $l_{final}$ ,  $T_{act}$ , and  $\varepsilon_{act}$  (Video S01). We then repeated this procedure for different values of  $\sigma_{act}$  (from 0 to ~20MPa) and  $T_{prog}$  (relative to  $T_g$ ) (Figures S13-15). All three SMPs exhibited good shape fixity (~0.9) and shape recovery (~0.9) for  $\sigma_{act} = 0$  (Figure S16). Moreover, a clear nonlinear relationship between  $\sigma_{act}$  and  $\varepsilon_{act}$  is observed (Figure 4B), in which  $\varepsilon_{act}$  monotonically decreases from ~0.6 to 0 as  $\sigma_{act}$  increases from 0 to ~13-18MPa for all three polymers. At low  $\sigma_{act}$ ,  $\varepsilon_{act}$  approaches its maximum value of 0.75 (for an initial strain of 300%).

Since the work done by the polymer is given by  $W = \sigma_{act} \varepsilon_{act}$ , the area under the solid line in **Figure 4B** corresponds to the measured energy density (in MJ/m<sup>3</sup>) for each polymer. In addition, the x-intercept and y-intercept of the plot correspond to the commonly reported values of recovery stress,  $\sigma_{r,max}$  and recovery strain,  $\varepsilon_{r,max}$ , respectively. A common assumption is that the ideal energy density is given by:

$$E_{ideal} = \frac{1}{2} \sigma_{r,max} \varepsilon_{r,max} \tag{3}$$

This equation assumes ideal Hookean spring behavior and is analogous to calculating the area under the dashed lines plotted in **Figure 4B**. Thus, the difference between the measured energy density from the ideal energy density allows us to quantitatively characterize the extent to which each polymer network deviates from an ideal spring (**Figure 4C**, **Note S1**). The ideal energy densities ( $\sim$ 5-6 MJ/m³) are approximately twice that of the measured energy densities ( $\sim$ 2-3 MJ/m³). Comparing both the ideal energy densities and the recovery stresses of the  $x_{MPU} = 1.0, 0.9,$  and 0.7 polymers with other previously

reported shape memory polymers highlights the improved performance of the SMPs in this work, which is enabled by the use of strain-induced supramolecular structures (**Figure 4D**, **Table S4**)<sup>[4,13,24,28,41–58]</sup>. Furthermore, the low energy density from previously reported shape memory polymers hindered the realization of SMASH of large-sized damage areas, with the most significant damage dimension being below 1 mm. (**Figure 4D**, **Table S5**)<sup>[15,16,23,26,37,54,59–71]</sup>

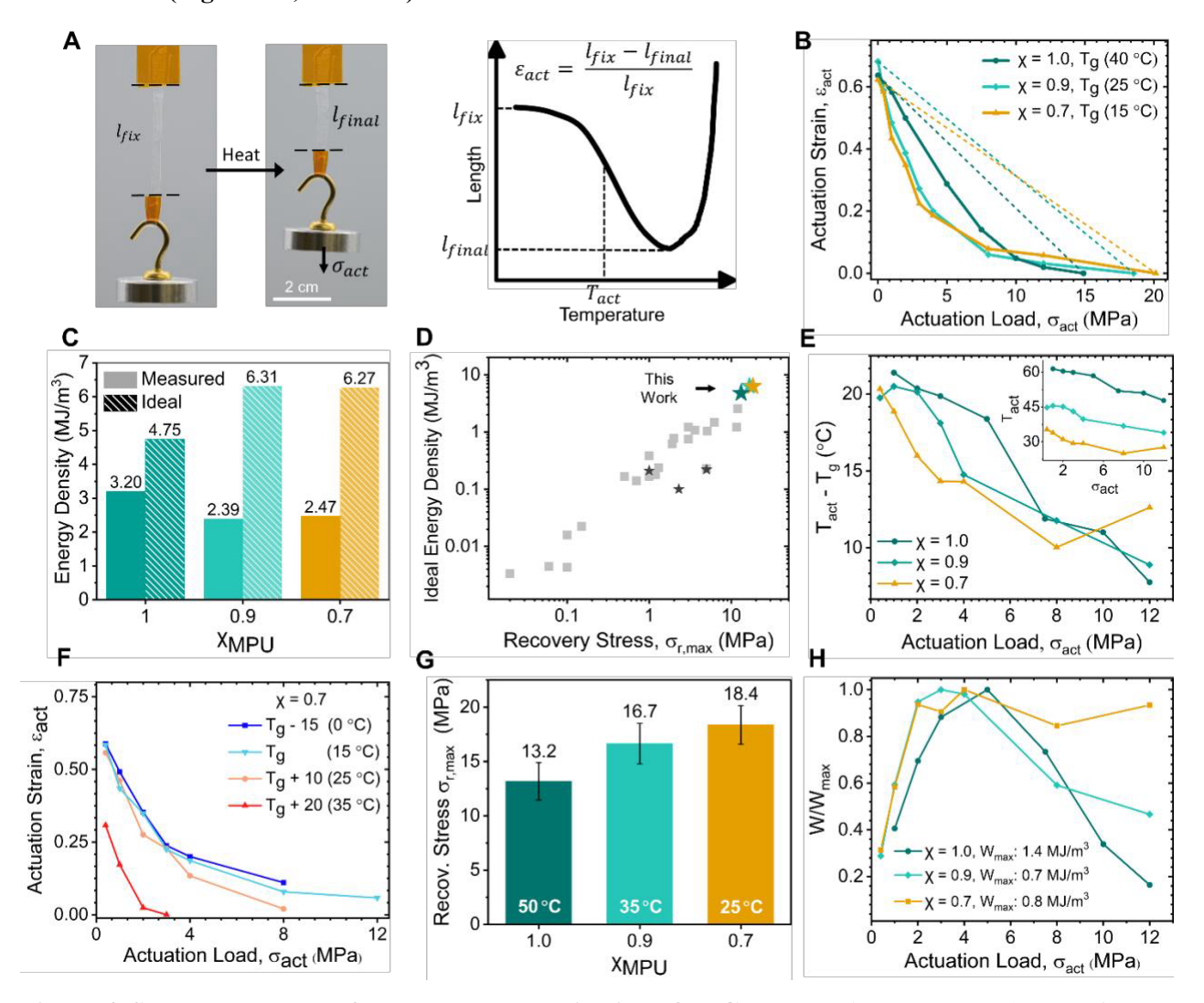


Figure 4. Shape memory performance characterization of PPG-MPU<sub>x</sub>-PA<sub>1-x</sub> polymers ( $x_{MPU} = 1$ , **0.9, 0.7)** A) Demonstration of shape memory performance characterization using a PPG-MPU<sub>0.7</sub>-PA<sub>0.3</sub> film with  $l_{fix}$ ,  $l_{final}$ , and  $\sigma_{act}$  marked (left). Illustration of length versus temperature during heating (right). The material initially contracts from  $l_{fix}$  to  $l_{final}$  as temperature increases. B) Actuation strain versus actuation load of  $x_{MPU} = 0.7$  (yellow),  $x_{MPU} = 0.9$  (teal), and  $x_{MPU} = 1.0$  (dark teal) (n = 1) C) Measured energy density (area under solid line in C, solid left) and ideal energy density  $E_{ideal}$  (area under dashed line in C, striped right) for the  $x_{MPU} = 1.0$ , 0.9, and 0.7 polymers. D) Ideal energy density  $E_{ideal}$  verus recovery stress of  $x_{MPU} = 0.7$ ,  $x_{MPU} = 0.9$ ,  $x_{MPU} = 1.0$  and previous reported SMPs

(grey square) and SMASH SMPs (black box). **E)** Actuation temperature shifted by  $T_g$  versus actuation load for the  $x_{\text{MPU}} = 1.0$ , 0.9, and 0.7 polymers. **F)** Actuation strain versus actuation load of PPG-MPU<sub>0.7</sub>-PA<sub>0.3</sub> with programming temperatures of  $T_{prog} = T_g - 15$  °C = 0 °C (blue),  $T_{prog} = T_g = 15$  °C (light blue),  $T_{prog} = T_g + 10$  °C = 25 °C (orange), and  $T_{prog} = T_g + 20$  °C = 35 °C. (red). **G)** Recovery stress values for  $x_{\text{MPU}} = 1.0$ , 0.9, and 0.7 films initially strained to 300% (n = 2). Temperature numbers indicated in the figure represent the temperature where the maximum stress was observed. **H)** Normalized actuation work at a specific  $\sigma_{act}$  versus actuation load of  $x_{\text{MPU}} = 1.0$ -0.7.

We also investigated how  $T_{act}$  changes with  $T_g$  for PPG-MPU<sub>1.0</sub>, PPG-MPU<sub>0.9</sub>-PA<sub>0.1</sub>, and PPG-MPU<sub>0.7</sub>-PA<sub>0.3</sub>. All polymers were observed to actuate 10-20 °C above their respective  $T_g$ , with higher temperatures required for actuation for higher  $\sigma_{act}$  (**Figure 4E**). This finding suggests that all three polymers actuate via a similar mechanism, in which the strain-induced supramolecular assemblies are disrupted 10-20 °C above  $T_g$ , with higher temperatures needed to disrupt the assemblies held at higher stress, since the stress acts to stabilize the stretched chain state. Moreover, these results highlight the importance of incorporating PA units into the polymer backbone, which adjusts  $T_g$ , and subsequently tunes  $T_{act}$  while maintaining high energy density as shown in **Figure 4C**. Thus, PPG-MPU<sub>1.0</sub> actuates at 50-60 °C, PPG-MPU<sub>0.9</sub>-PA<sub>0.1</sub> at 35-45 °C, and PPG-MPU<sub>0.7</sub>-PA<sub>0.3</sub> at 25-35 °C. The lower  $T_{act}$  for PPG-MPU<sub>0.9</sub>-PA<sub>0.1</sub> and PPG-MPU<sub>0.7</sub>-PA<sub>0.3</sub> can be used in situations where actuation near physiological temperature is desired, such as in biomedical devices or wearable electronics.

We also investigated the effect of  $T_{prog}$  on shape memory performance (**Figure 4F**). When initially strained at 20 °C above its  $T_g$ , PPG-MPU<sub>0.7</sub>-PA<sub>0.3</sub> showed significantly reduced actuation strain. We attribute this decrease in performance to the inability to form supramolecular structures at higher temperatures, supported by the previous data (**Figure 4E**) that suggests the strain-induced supramolecular structures begin to dissociate at  $T_g + 20$  °C and cause actuation even under the highest loads tested. In addition, we found that decreasing  $T_{prog}$  below  $T_g$  did not change the energy density curve. We initially hypothesized that the introduction of PA units, which are weaker hydrogen bonding units, into the polymer backbone would decrease the recovery stress  $\sigma_{r,max}$ . However, we observed the opposite effect, with PPG-MPU<sub>1.0</sub> showing the lowest  $\sigma_{r,max}$  of  $13.2 \pm 1.72$  MPa and PPG-MPU<sub>0.7</sub>-PA<sub>0.3</sub> showing the highest  $\sigma_{r,max}$  of  $18.4 \pm 1.76$  MPa (**Figure 4G**, **Figure S17**). This trend can be understood by considering how the network storage modulus of the polymers varies with temperature. While all three polymers exhibit actuation 10-20 °C above  $T_g$  (**Figure 4E**), the storage modulus of PPG-MPU<sub>0.7</sub>-PA<sub>0.3</sub> are stable

and higher up to  $T_g + 20$  °C (**Figure 3B**). Since the recovery stress reaches a maximum for all of the polymers at temperatures above  $T_g + 10$  °C, this decay in the network strength is likely responsible for the decreased recovery stress of PPG-MPU<sub>1.0</sub>.

Finally, we also calculated the actual work output ( $W = \varepsilon_{act} \sigma_{act}$ ) for different  $\sigma_{act}$  for each polymer, which is particularly important for the development of practical devices, which commonly actuate against a constant force. **Figure 4H** shows the normalized plot of  $\frac{W}{W_{max}}$  versus  $\sigma_{act}$ . While PPG-MPU<sub>1.0</sub> has the highest  $W_{max}$  compared to PPG-MPU<sub>0.9</sub>-PA<sub>0.1</sub> and PPG-MPU<sub>0.7</sub>-PA<sub>0.3</sub>, PPG-MPU<sub>0.7</sub>-PA<sub>0.3</sub> can maintain its maximum work output at higher loads. We attribute this improved performance to the more stable network modulus of PPG-MPU<sub>0.7</sub>-PA<sub>0.3</sub> at higher temperatures (**Figure 3B**), since actuation at higher loads occurs at  $T_q + 20$  °C (**Figure 4E**).

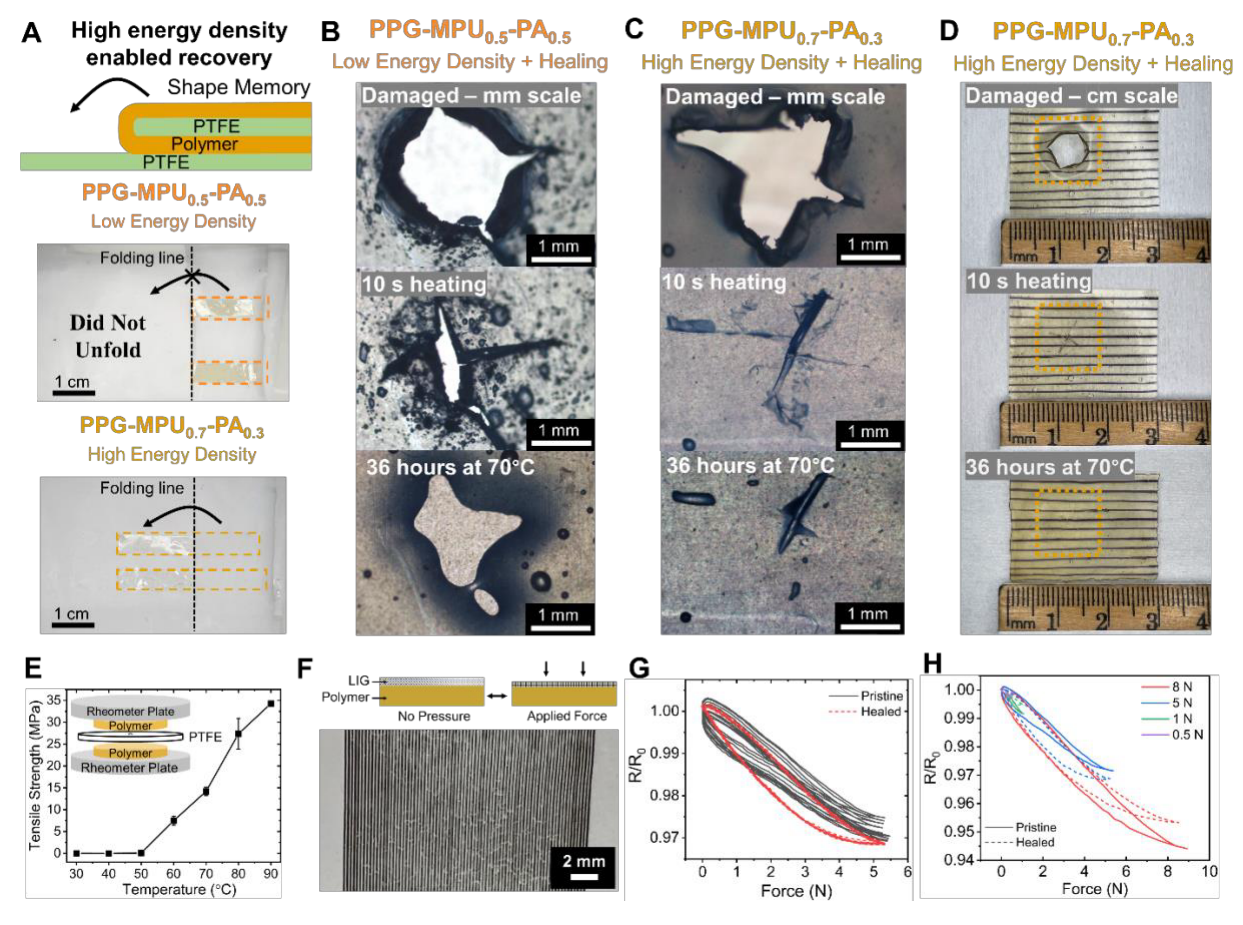


**Figure 5. Shape-memory-assisted self-healing (SMASH) of macroscopic punctures and pressure sensor demonstration using PPG-MPU<sub>0.7</sub>-PA<sub>0.3</sub>. A)** Films of PPG-MPU<sub>0.5</sub>-PA<sub>0.5</sub> (control, low energy density at R.T., 0.06 mm thickness) and PPG-MPU<sub>0.7</sub>-PA<sub>0.3</sub> (high energy density at R.T., 0.06 mm thickness) were folded (at 50 % of their initial length, 3.0 cm) onto a PTFE sheet and then heated to

measure their shape memory recovery (i.e., unfolding) back to their initial state. Only the high energy density SMP, PPG-MPU<sub>0.7</sub>-PA<sub>0.3</sub>, is able to unfold when heated. **B)** Image of a punctured PPG-MPU<sub>0.5</sub>- $PA_{0.5}$  film (control, low energy density and healing) with a 1.5 mm diameter hole created from twisting a scalpel into the polymer after damage (top), after 10 s of heating with a heat gun from 30 cm distance (middle), and after 36 hours at 70 °C (bottom). C) Image of a punctured PPG-MPU<sub>0.7</sub>-PA<sub>0.3</sub> film (high energy density and healing) with a 2 mm diameter hole created from twisting a scalpel into the polymer after damage (top), after 10s of heating with a heat gun from 30 cm distance (middle), and after 36 hours at 70 °C (bottom). D) Image of a PPG-MPU<sub>0.7</sub>-PA<sub>0.3</sub> film (marked with a marker to improve visibility of the damage) with a 1 cm diameter hole created from a scalpel and a screwdriver into the polymer after damage (top), after 10s of heating with a heat gun from 30 cm distance (middle), and after annealing for 36 hours at 70 °C (bottom). E) Self-healing data measured by rheometer for PPG-MPU<sub>0.7</sub>-PA<sub>0.3</sub> showing the recovery in tensile strength for different temperatures with a constant healing time of 30 minutes. The inset shows a schematic of the measurement set-up in which two pieces of polymer are healed with a controlled contact area defined by a PTFE sheet with a hole in it. F) Image of PPG-MPU<sub>0.7</sub>-PA<sub>0.3</sub> patterned with laser-induced graphene (LIG) lines transferred from polyimide films. G) Cyclic pressure sensor data up to 5 N before (black solid line) and after (red dashed line) self-healing at 70 °C for 24 hours for 10 cycles. H) Pressure sensor performance before (solid lines) and after (dashed lines) selfhealing at 70 °C for 24 hours for different loads.

We next sought to demonstrate the application of these high energy density shape memory polymers and hypothesized that the combination of high energy density shape memory and self-healing properties could enable recovery from large macroscopic damages through a combination of autonomous self-closing and self-healing. We first demonstrated the importance of the high energy density in the process of shape recovery after sample damage by folding a control sample of PPG-MPU<sub>0.5</sub>-PA<sub>0.5</sub> (low energy density) and a sample of PPG-MPU<sub>0.7</sub>-PA<sub>0.3</sub> (high energy density). Without sufficient energy density, the low energy density control sample failed to return to the original shape (**Figure 5A**).

The unfolding of a folded or bent film to its original state is similar to the SMASH process of recovering from a large damage and here serves as a proxy to identify both which polymers could exhibit SMASH behavior and why SMASH behavior improves with higher energy density. To a first approximation, the size of the folded or bent region scales with the perimeter of the damage (proportional to the hole radius) while the size of the region being lifted scales with the area of the damage (proportional to the hole radius squared). Thus, for larger hole sizes, more work must be done by the damaged perimeter to bring the pieces back into contact. To demonstrate this, based on the experiment shown in Figure 5A, we also

folded PPG-MPU<sub>0.7</sub>-PA<sub>0.3</sub> films at different positions and measured its ability to unfold itself when heated, suggesting a maximum hole radius for puncture recovery of  $\sim$ 2.1cm (**Figure S18**).

These results suggested the PPG-MPU<sub>0.5</sub>-PA<sub>0.5</sub> would be unsuitable for SMASH, which we tested by damaging a sample of PPG-MPU<sub>0.5</sub>-PA<sub>0.5</sub>, with a scalpel to generate a 1-2 mm hole (Figure 5B). The damaged area remained unchanged after annealing at 70 °C for 36 hours (Figure 5B). On the other hand, the folded film experiments suggested that PPG-MPU<sub>0.7</sub>-PA<sub>0.3</sub> would have sufficient energy density to exhibit SMASH behavior at large length scales. Indeed, after being punctured to form a 1-2 mm hole, PPG-MPU<sub>0.7</sub>-PA<sub>0.3</sub> was able to self-close the puncture within 10 seconds of heating, benefitted from the high energy density together with the excellent shape recovery of ~ 90%. (Video S2). The punctured film, after self-closing, was fully healed after annealing at 70 °C for 36 hours, despite having a higher terminal flow temperature of 80 °C and thus slower diffusive self-healing than PPG-MPU<sub>0.5</sub>-PA<sub>0.5</sub> (Figure 5C, Figure S19). When the healed sample was subsequently subjected to strain, the film broke far away from the healing location in the undamaged region and exhibited similar mechanical properties to the pristine film, suggesting it had fully recovered (Figure S19). To further demonstrate the robustness of the SMASH behavior in our high energy density SMP, we increased the damage area to a >1 cm hole and showed that the material was also able to fully heal (Figure 5D). While SMASH has been used to heal minor scratches and notches (Table S5), the significantly higher energy density of our SMP, compared to previously reported SMPs, enables self-healing of larger punctures of centimeter size, which was previously unachievable.

We characterized the diffusive self-healing behavior by allowing PPG-MPU<sub>0.7</sub>-PA<sub>0.3</sub> to heal through a small hole on a PTFE film on a rheometer for 30 minutes, following a previously reported procedure, enabling us to quantify the self-healing ability under different temperatures (**Figure 5E**, **Figure S19**). The polymer demonstrated highly efficient self-healing at elevated temperatures, as evidenced by the high tensile strength shown for temperatures at and above 70 °C, consistent with the terminal flow temperature of 80 °C (**Figure 3A**). The SMASH behavior of the PPG-MPU<sub>0.7</sub>-PA<sub>0.3</sub> was also shown to be reliable and reproducible - when the material was punctured in a consistent way multiple times, over 90% of the punctures were healed successfully (**Figure S19**). This high-level of the SMASH capability makes PPG-MPU<sub>0.7</sub>-PA<sub>0.3</sub> an ideal candidate for stretchable electronics and soft robotics. To demonstrate this capability, we patterned laser-induced-graphene onto the PPG-MPU<sub>0.7</sub>-PA<sub>0.3</sub>, to fabricate an array of force sensors (**Figure 5F**). We demonstrate the excellent cyclability of resistance change for a single sensor and show that the sensor maintains the same performance after being cut and self-healed for 24 hours at 70 °C

(**Figure 5G**). Furthermore, the sensor also shows sensitivity across a wide force range, from 0.5 N to 8 N (**Figure 5H**).

### DISCUSSION AND CONCLUSION

This work demonstrates the use of high energy density shape memory polymers for self-healing films that can recover from large, macroscopic punctures and tears. Importantly, this SMASH capability is achieved by tuning the actuation and self-healing temperatures of periodic dynamic polymers, which form strain-induced supramolecular structures. We achieve this tunability by substituting strong hydrogen bonding polyurea units with weaker polyamide units to control the glass transition temperature of the bulk films. In addition, this research presents a detailed methodology to measure SMP energy density and deviation from ideal spring-like behavior, which can be used for other SMP materials. The combination of self-healing and shape memory effects in these materials allows them to repair large structural damages without the need for human intervention and may enable SMPs to have broader applications in wearable soft electronics and medical devices.

### **EXPERIMENTAL SECTION**

#### Materials

Diamine-terminated poly(propylene glycol) ( $H_2N$ -PPG-NH<sub>2</sub>) macromonomers were obtained from Huntsman (Jeffamine D400,  $M_n$ = 0.4 kDa). All other chemicals and solvents were purchased from Sigma-Aldrich. All reagents were used as received without further purification.

# *Synthesis of PPG-MPU<sub>x</sub>-PA<sub>1-x</sub> polymers*

Diamine-terminated poly(propylene glycol) ( $H_2N$ -PPG-NH<sub>2</sub>) macromonomers (Jeffamine D400,  $M_n$ = 0.4 kDa) were placed at 90 °C under vacuum for 2 hours to remove trace water. Using PPG-MPU<sub>0.7</sub>-PA<sub>0.3</sub> as an example, terephthaloyl chloride (TC, 148.7 mg, 0.7 mmol) and 4,4'-Methylenebis(phenyl isocyanate) (MDI, 427.8 mg, 1.9 mmol) were dissolved in 10mL of dichloromethane (DCM) and stirred in an ice bath.  $H_2N$ -PPG-NH<sub>2</sub> (1.0 g, 2.50 mmol) and triethylamine (TEA) (~0.7 g, 6.9 mmol) were added in another round-bottom flask and dissolved in DCM (10 mL) in an ice bath. The molar ratio of each chemical was calculated by 1.0:1.05 amine:isocyanate functional groups and greater than 1:2 TC:TEA. The solution of  $H_2N$ -PPG-NH<sub>2</sub> and TEA solution was slowly added to the flask with TC and MDI. After allowing the ice to melt to reach room temperature slowly, the reacting mixture was stirred at room temperature for 48 hours under the nitrogen environment. The solution was evaporated to viscous liquid and hexane was added slowly to precipitate the polymer. The polymer was rinsed three times in hexane. To remove salt, the polymer was dissolved in methanol and precipitated in water three times. The polymer was rinsed with water and dried at 100 °C *in vacuo* for 24 hours.

### Size exclusion chromatography

Size exclusion chromatography (SEC) analysis was performed using a Tosoh EcoSEC Ambient (Room Temperature)-GPC equipped with two TSK gel GPC columns (G3000Hhr and G4000Hhr; 7.8 mm I.D. x 30 cm, 5  $\mu$ m) calibrated with a conventional calibration curve using monodisperse polystyrene standards. Tetrahydrofuran (THF) (40 °C) was used as a carrier solvent at the flow rate of 1.0 mL/min. Samples were prepared at 1 mg/mL in THF, except for PPG-MPU<sub>1.0</sub>, which was first dissolved in CHCl<sub>3</sub> (5 mg/mL) and then diluted with THF to reach a concentration of around 1 mg/mL.

## Mechanical characterization methods

Room temperature tensile tests were conducted on an Instron 5565 Instrument at a constant strain rate of 200 % per minute. Rectangular samples with approximate dimensions of 10 mm x 4 mm x 0.1 mm were cut from the substrate and loaded onto the extensometer with pressurized grips using double-sided tape to improve sample-grip adhesion and prevent slipping as needed.

## Rheological characterization methods

Dynamic mechanical analyses were conducted using an Ares G2 Rheometer with an 8 mm parallel plate set-up in a temperature-controlled convection oven. Samples were cut into 8mm diameter discs with a thickness of  $\sim$ 0.1 mm. Frequency sweep tests were collected from 100 rad/s to 0.1 rad/s at designated temperatures with an applied strain of 1% under a constant axial force of 0.1 N. Temperature sweeps were performed in 10 °C steps with a wait time of 180 s between steps to allow the sample temperature to equilibrate. For MPU fractions above  $x_{\text{MPU}} = 0.5$ , frequency sweeps at temperatures below 70 °C were taken with an applied strain of 0.1% to remain with the linear viscoelastic regime, and temperature steps were taken every 5 °C. To ensure full contact between the sample and the plates, a pre-conditioning step was used, in which the sample was heated above terminal flow and a frequency sweep was performed from 100 rad/s to 0.1 rad/s under a small force between 0.1-0.5 N.

## Differential scanning calorimetry

Differential scanning calorimetry (DSC) was conducted using a TA instruments Q2000 DSC. Approximately 10 mg of polymer were placed in sealed aluminum pans and lids. Samples were ramped from -90 °C to 150 °C at a rate of 10 °C/min. Glass transition temperatures were extracted using TA TRIOS software.

## *Small-angle x-ray scattering methods*

Small-angle x-ray scattering (SAXS) was conducted in transmission mode on bulk polymer films at beamline 4-2 at Stanford Synchrotron Radiation Lightsource (SSRL) of SLAC National Accelerator Laboratory (SLAC, Menlo Park, CA). Bulk polymer films were tested as free-standing films with a thickness of 0.1 mm. The x-ray wavelength was 0.827 Å (beam energy 15 keV) with a sample-to-detector distance of 3.512 m. The Pilatus 1M fast detector was used for 2D scattering data acquisition and reduction into 1D scattering intensity profiles was done using customized code at the beamline. For each sample, 10 frames of 1 second exposure were averaged to improve the signal-to-noise ratio. Measurements were performed in ambient air. All fitting was done using a dual annealing optimization method in Python.

# *X-ray diffraction analysis (XRD)*

X-ray diffraction analysis was conducted on a Bruker D8 Venture single-crystal X-ray diffractometer. The instrument was equipped with a micro-focus X-ray tube with a Cu-source (CuK $\alpha$ ,  $\lambda$  = 1.54178 Å) and equipped with a Photon 100 CMOS detector. The instrument was set up such that the polymer film

samples were mounted and centered perpendicular to the incident beam, and the detector was placed at  $2\theta$  = 0 ° at a sample-to-detector distance of 70 mm. Hot pressed bulk polymer films, with a thickness of ~ 10 um, of PPG-MPU<sub>1.0</sub>, PPG-MPU<sub>0.9</sub>-PA<sub>0.1</sub>, and PPG-MPU<sub>0.7</sub>-PA<sub>0.3</sub> were tested as unstrained samples. Similar films of PPG-MPU<sub>1.0</sub>, PPG-MPU<sub>0.9</sub>-PA<sub>0.1</sub>, and PPG-MPU<sub>0.7</sub>-PA<sub>0.3</sub> were strained to 600% on the DMA at their respective glass transition temperatures, which were placed in a Styrofoam box with dry ice to prevent actuation. The strained films were clamped to the mount rigidly during measurements. All XRD experiments were carried out at room temperature with static exposure time of 300 seconds each. All data were analyzed using Bruker Apex 4 software. 1D scattering intensity profiles were calculated by integrating 2D data of each strained sample from gamma of 165-170° (perpendicular to the strain) and 75-80° (parallel to the strain). FWHM data was analyzed using OriginPro Quickpeaks function on the smoothed plots.

## Atomic force microscopy experiments

Height and phase images were collected via atomic force microscopy (AFM) on a Nanoscope IIII Multimode AFM in tapping mode with Tap300Al-G probes (radius < 10 nm). All images and statistical distribution extraction were processed using Gwyddion software.

# *Self-healing experiments*

Self-healing experiment of bulk film: PPG-MPU<sub>0.7</sub>-PA<sub>0.3</sub> and PPG-MPU<sub>0.5</sub>-PA<sub>0.5</sub> were prepared by hotpressing at 100 °C for at least 5 minutes to achieve a thickness of approximately 0.3 mm. 16-gauge needles (diameter = 1.651 mm), surgical grade scalpels #11, or a screwdriver (diameter  $\sim$ 1 cm) were used as the sharp objects to create punctures on each film. The damaged films were gently heated using a heat gun placed 30 cm away for 10 seconds. All samples were placed on a clean surface (glass/PTFE film) without intervention and allowed to anneal in a 70 °C oven.

Self-healing experiments measured on rheometer: Two PPG-MPU $_{0.7}$ -PA $_{0.3}$  samples were placed on an Ares-G2 rheometer equipped with 25 mm parallel plate and a convection oven, and the samples were separated with a thin PTFE film that had a  $\sim$ 0.5 mm diameter hole in the center. Two samples were allowed to self-heal under a constant axial force of 0.1 N for 30 minutes at different temperatures. The degree of self-healing was measured as the parallel plates were pulled apart. The self-healing data at 90 °C consisted of only one data point because for other points the samples were completely healed and triggered the force limit on the instrument.

# Shape memory experiments

PPG-MPU<sub>1.0</sub>, PPG-MPU<sub>0.9</sub>-PA<sub>0.1</sub>, and PPG-MPU<sub>0.7</sub>-PA<sub>0.3</sub> were hot pressed between two PTFE thin films at 140 °C, 110 °C, and 100 °C, respectively, for at least 5 minutes for a thickness between 0.1 and 0.2 mm. The hot-pressed films were cut into strips approximately 2-3 mm wide and with a length at least three times their width. These films were loaded onto a TA Instruments Q800 Dynamic Mechanical Analyzer (DMA) equipped with tension film geometry. The shape memory test began by ramping temperature to a given temperature with a ramp rate of 2 °C/min. The film was strained to 300% at a strain rate of 50 %/min. The strained film was held at 300% strain for 30 minutes, after which it was allowed to self-relax under 0 MPa stress for 5 minutes. Following self-relaxation, the film was heated up to 100 °C with a heating rate of 5 °C/min.

## Recovery stress experiments

PPG-MPU<sub>1.0</sub>, PPG-MPU<sub>0.9</sub>-PA<sub>0.1</sub>, and PPG-MPU<sub>0.7</sub>-PA<sub>0.3</sub> films were prepared by the sample method mentioned in the Shape memory experiments section. These films were loaded on the tension film geometry in a TA Instrument Q800 DMA. First, the temperature was equilibrated to each sample's glass transition temperature. (40 °C, 25 °C, 15 °C for PPG-MPU<sub>1.0</sub>, PPG-MPU<sub>0.9</sub>-PA<sub>0.1</sub>, and PPG-MPU<sub>0.7</sub>-PA<sub>0.3</sub> respectively) The film was then strained to 300 % at a strain rate of 50 %/min and maintained at 300 % strain for 30 minutes. Subsequently, the film was allowed to self-relax under 0 MPa stress for 5 minutes. At the end of this period, the film's length was recorded, and the film was held at a constant length. All the steps above were carried out at each polymer's respective glass transition temperature. As the film was heated to 100 °C with a heating rate of 5 °C/min, the stress was monitored. The highest stress value was reported as the recovery stress.

# Film folding experiments

Two PPG-MPU<sub>0.7</sub>-PA<sub>0.3</sub> films and four PPG-MPU<sub>0.5</sub>-PA<sub>0.5</sub> were prepared by hot pressing at 110 °C (PPG-MPU<sub>0.7</sub>-PA<sub>0.3</sub>) or 100 °C (PPG-MPU<sub>0.5</sub>-PA<sub>0.5</sub>) for 5 minutes then cut into similar rectangle sizes of 30 x 4 x 0.06 mm. Each film weighs ~20 mg. The films were held between two sheets of PTFE films to prevent any adhesion, then the films can be folded over onto the PTFE using a pair of tweezers. The setup and process's sideview can be found in Figure S18. Then the folded film was be placed onto an 80 °C hotplate to initiate the shape memory process. The strain and compression caused by the folding process will attempt to lift the folded part against the gravity back to the flat shape. The length of the folded part is free to move while the section of the folding crease is held in place.

*Self-healing pressure sensor demonstration* 

Films of PPG-MPU<sub>0.7</sub>-PA<sub>0.3</sub> were prepared by drop casting 100 mg/mL solutions in CHCl<sub>3</sub> onto SiO<sub>2</sub> wafers treated with a monolayer of octadecyltrichlorosilane (OTS) to allow for easy removal of the film and dried for over 12 h at room temperature and then again at 70 °C for at least 24 h. Laser-induced graphene (LIG) was prepared by laser engraving of a polyimide film (Kapton®, Electrical-Grade, obtained from McMASTER-CARR) by an Epilog Fusion M2 CO2 Laser following a reported method.<sup>[74]</sup> A laser power of 7.5 W and a raster speed of 30% were used.

The pressure sensor was prepared by first transferring LIG from polyimide (PI) film onto a film of PPG-MPU<sub>0.7</sub>-PA<sub>0.3</sub> by hot-pressing the films at 70 °C for 1 minute. Copper electrodes were connected to the LIG using silver paste and cured overnight at 70 °C. Resistance measurements for the pressure sensor were done with a Keithley 2601B Source Meter, sourcing 10 mA and a simple voltage divider setup. Forces between 0.5-10 N were cycled during testing. The self-healing of the sensor was checked by cutting the device in half with a blade, healing the electrodes at 70 °C for 24 hours, and then remeasuring the sensor performance.

#### **ACKNOWLEDGEMENTS**

This work is in part supported by the Army Research Office (ARO) Materials Design Program (Grant no. W911NF-21-1-0092) and the Ford Motor Company under the Ford-Stanford Alliance. Authors are grateful for the discussions with Haibo Zhao, Jaewon Yoon, Janice Tardiff, and Xiaojiang Wang from the Ford Research team. CBC acknowledges support from the Department of Defense via a National Defense Science & Engineering Graduate Fellowship. L.M. acknowledges funding through the Walter Benjamin Fellowship Programme by the Deutsche Forschungsgemeinschaft (DFG 456522816). Part of characterization was performed at the Stanford Nano Shared Facilities (SNSF), supported by the National Science Foundation under Award ECCS-1542152. SAXS experiments were conducted at Stanford Synchrotron Radiation Lightsource within the SLAC National Accelerator Laboratory supported by the U.S. Department of Energy, Office of Science, Office of Basic Energy Sciences under Contract No. DE-AC02-76SF00515.

## REFERENCES

- [1] A. Lendlein, S. Kelch, *Angew. Chem. Int. Ed.* **2002**, *41*, 2034.
- [2] J. Hu, Y. Zhu, H. Huang, J. Lu, Prog. Polym. Sci. 2012, 37, 1720.
- [3] A. Lendlein, O. E. C. Gould, *Nat. Rev. Mater.* **2019**, *4*, 116.
- [4] C. B. Cooper, S. Nikzad, H. Yan, Y. Ochiai, J.-C. Lai, Z. Yu, G. Chen, J. Kang, Z. Bao, *ACS Cent. Sci.* **2021**, *7*, 1657.
- [5] T. Wan, B. Wang, Q. Han, J. Chen, B. Li, S. Wei, *Appl. Mater. Today* **2022**, *29*, 101665.

- [6] L. Yang, J. Lou, J. Yuan, J. Deng, RSC Adv. 2021, 11, 28838.
- [7] N. Besse, S. Rosset, J. J. Zarate, H. Shea, *Adv. Mater. Technol.* **2017**, *2*, 1700102.
- [8] J. M. McCracken, B. R. Donovan, T. J. White, *Adv. Mater.* **2020**, *32*, 1906564.
- [9] M. D. Hager, S. Bode, C. Weber, U. S. Schubert, *Prog. Polym. Sci.* **2015**, 49–50, 3.
- [10] M. Anthamatten, S. Roddecha, J. Li, Macromolecules 2013, 46, 4230.
- [11] C. B. Cooper, Z. Bao, Acc. Mater. Res. 2022, 3, 948.
- [12] W. Liu, Y. He, J. Leng, ACS Appl. Polym. Mater. 2022, 4, 6092.
- [13] W. Liu, Y. He, J. Leng, ACS Appl. Mater. Interfaces 2023, 15, 2163.
- [14] X. Zheng, Y. Chen, C. Chen, Z. Chen, Y. Guo, H. Li, H. Liu, *J. Mater. Chem. B* **2021**, *9*, 7371.
- [15] E. D. Rodriguez, X. Luo, P. T. Mather, ACS Appl. Mater. Interfaces 2011, 3, 152.
- [16] Y. Yang, D. Davydovich, C. C. Hornat, X. Liu, M. W. Urban, *Chem* **2018**, *4*, 1928.
- [17] S. Bonardd, M. Nandi, J. I. Hernández García, B. Maiti, A. Abramov, D. Díaz Díaz, *Chem. Rev.* **2023**, *123*, 736.
- [18] Z. Li, R. Yu, B. Guo, ACS Appl. Bio Mater. **2021**, 4, 5926.
- [19] D. Tang, L. Zhang, X. Zhang, L. Xu, K. Li, A. Zhang, *ACS Appl. Mater. Interfaces* **2022**, *14*, 1929.
- [20] M. Khatib, O. Zohar, H. Haick, Adv. Mater. 2021, 33, 2004190.
- [21] M. Khatib, O. Zohar, W. Saliba, H. Haick, Adv. Mater. 2020, 32, 2000246.
- [22] R. R. Kohlmeyer, M. Lor, J. Chen, *Nano Lett.* **2012**, *12*, 2757.
- [23] B. T. Michal, C. A. Jaye, E. J. Spencer, S. J. Rowan, ACS Macro Lett. 2013, 2, 694.
- [24] T. Lin, Z. Tang, B. Guo, ACS Appl. Mater. Interfaces 2014, 6, 21060.
- [25] C. C. Hornat, M. W. Urban, *Nat. Commun.* **2020**, *11*, 1.
- [26] X. Luo, P. T. Mather, ACS Macro Lett. 2013, 2, 152.
- [27] J. Kang, D. Son, G.-J. N. Wang, Y. Liu, J. Lopez, Y. Kim, J. Y. Oh, T. Katsumata, J. Mun, Y. Lee, L. Jin, J. B.-H. Tok, Z. Bao, *Adv. Mater.* **2018**, *30*, 1706846.
- [28] D. M. Krajovic, M. Anthamatten, ACS Appl. Polym. Mater. 2021, 3, 2082.
- [29] H. M. Park, M. Ismael, H. Takaba, Y. T. Lee, J. Membr. Sci. 2022, 645, 120175.
- [30] J. C. Worch, A. C. Weems, J. Yu, M. C. Arno, T. R. Wilks, R. T. R. Huckstepp, R. K. O'Reilly, M. L. Becker, A. P. Dove, *Nat. Commun.* 2020, 11, 3250.
- [31] P. C. Je, M. T. Sultan, C. P. Selvan, S. Irulappasamy, F. Mustapha, A. A. Basri, S. N. A. Safri, *J. Mater. Res. Technol.* **2020**, *9*, 7370.
- [32] S. Wang, M. W. Urban, *Nat. Rev. Mater.* **2020**, *5*, 562.
- [33] E. B. Stukalin, L.-H. Cai, N. A. Kumar, L. Leibler, M. Rubinstein, *Macromolecules* **2013**, 46, 7525.
- [34] D. Döhler, J. Kang, C. B. Cooper, J. B.-H. Tok, H. Rupp, W. H. Binder, Z. Bao, *ACS Appl. Polym. Mater.* **2020**, DOI 10.1021/acsapm.0c00755.
- [35] C. B. Cooper, S. E. Root, L. Michalek, S. Wu, J.-C. Lai, M. Khatib, S. T. Oyakhire, R. Zhao, J. Qin, Z. Bao, *Science* **2023**, *380*, 935.
- [36] C. C. Hornat, M. W. Urban, *Prog. Polym. Sci.* **2020**, *102*, 101208.
- [37] E. Wornyo, K. Gall, F. Yang, W. King, *Polymer* **2007**, 48, 3213.
- [38] D. J. Skrovanek, S. E. Howe, P. C. Painter, M. M. Coleman, *Macromolecules* 1985, 18, 1676.
- [39] J. Mattia, P. Painter, *Macromolecules* **2007**, *40*, 1546.
- [40] C. E. R. Edwards, D. J. Mai, S. Tang, B. D. Olsen, *Phys. Rev. Mater.* **2020**, *4*, 015602.
- [41] Q. Yang, G. Li, J. Polym. Sci. Part B Polym. Phys. **2014**, 52, 1429.

- [42] P. Zhang, G. Li, J. Polym. Sci. Part B Polym. Phys. 2013, 51, 966.
- [43] Z. Xu, Y.-B. Liu, D.-W. Wei, R.-Y. Bao, Y. Wang, K. Ke, W. Yang, ACS Appl. Mater. Interfaces 2023, 15, 12423.
- [44] W. Wang, P. Ping, X. Chen, X. Jing, Eur. Polym. J. 2006, 42, 1240.
- [45] N. Fritzsche, T. Pretsch, Macromolecules 2014, 47, 5952.
- [46] Y. Meng, J. Jiang, M. Anthamatten, J. Polym. Sci. Part B Polym. Phys. 2016, 54, 1397.
- [47] N. A. Nguyen, K. M. Meek, C. C. Bowland, S. H. Barnes, A. K. Naskar, *Macromolecules* **2018**, *51*, 115.
- [48] C. L. Lewis, Y. Meng, M. Anthamatten, Macromolecules 2015, 48, 4918.
- [49] H. Kim, J. M. Boothby, S. Ramachandran, C. D. Lee, T. H. Ware, *Macromolecules* **2017**, *50*, 4267.
- [50] K. M. Lee, T. J. Bunning, T. J. White, Adv. Mater. 2012, 24, 2839.
- [51] J.-Q. Li, W.-S. Li, W.-T. Zhang, S. Zhu, C.-Y. Luo, W.-S. Liu, L.-Y. Zhang, *Chin. J. Polym. Sci.* **2023**, DOI 10.1007/s10118-023-2911-9.
- [52] M. O. Saed, C. P. Ambulo, H. Kim, R. De, V. Raval, K. Searles, D. A. Siddiqui, J. M. O. Cue, M. C. Stefan, M. R. Shankar, T. H. Ware, Adv. Funct. Mater. 2019, 29, 1806412.
- [53] M. Tian, W. Gao, J. Hu, X. Xu, N. Ning, B. Yu, L. Zhang, *ACS Appl. Mater. Interfaces* **2020**, *12*, 6426.
- [54] M. Burnworth, L. Tang, J. R. Kumpfer, A. J. Duncan, F. L. Beyer, G. L. Fiore, S. J. Rowan, C. Weder, *Nature* **2011**, *472*, 334.
- [55] Z. Fang, N. Zheng, Q. Zhao, T. Xie, ACS Appl. Mater. Interfaces 2017, 9, 22077.
- [56] J. Li, J. A. Viveros, M. H. Wrue, M. Anthamatten, Adv. Mater. 2007, 19, 2851.
- [57] L. Jiang, Z. Liu, Y. Lei, Y. Yuan, B. Wu, J. Lei, ACS Appl. Polym. Mater. 2019, 1, 3261.
- [58] G. Zhang, Q. Zhao, W. Zou, Y. Luo, T. Xie, Adv. Funct. Mater. 2016, 26, 931.
- [59] B. A. Nelson, W. P. King, K. Gall, *Appl. Phys. Lett.* **2005**, *86*, 103108.
- [60] G. Rivero, L.-T. T. Nguyen, X. K. D. Hillewaere, F. E. Du Prez, *Macromolecules* **2014**, 47, 2010.
- [61] N. Van Herck, F. E. Du Prez, *Macromolecules* **2018**, *51*, 3405.
- [62] X. Wang, J. Xu, Y. Zhang, T. Wang, Q. Wang, S. Li, Z. Yang, X. Zhang, *Nat. Commun.* **2023**, *14*, 4712.
- [63] Y. Yang, M. W. Urban, *Polym. Chem.* **2016**, *8*, 303.
- [64] X. Xiao, T. Xie, Y.-T. Cheng, J. Mater. Chem. 2010, 20, 3508.
- [65] Y. Chen, X. Zhao, Y. Li, Z.-Y. Jin, Y. Yang, M.-B. Yang, B. Yin, *J. Mater. Chem. C* **2021**, *9*, 5515.
- [66] B. Zhang, W. Zhang, Z. Zhang, Y.-F. Zhang, H. Hingorani, Z. Liu, J. Liu, Q. Ge, ACS Appl. Mater. Interfaces 2019, 11, 10328.
- [67] J. Chen, D. Sun, T. Gu, X. Qi, J. Yang, Y. Lei, Y. Wang, *Compos. Sci. Technol.* **2022**, *217*, 109123.
- [68] F. Orozco, M. Kaveh, D. S. Santosa, G. M. R. Lima, D. R. Gomes, Y. Pei, R. Araya-Hermosilla, I. Moreno-Villoslada, F. Picchioni, R. K. Bose, *ACS Appl. Polym. Mater.* **2021**, *3*, 6147.
- [69] L. Amornkitbamrung, S. Leungpuangkaew, T. Panklang, C. Jubsilp, S. Ekgasit, S. H. Um, S. Rimdusit, *J. Sci. Adv. Mater. Devices* **2022**, *7*, 100446.
- [70] W. Yan, Y. Ding, R. Zhang, X. Luo, P. Sheng, P. Xue, J. He, *Polymer* **2022**, *239*, 124436.
- [71] W. Alabiso, T. Manuel Hron, D. Reisinger, D. Bautista-Anguís, S. Schlögl, *Polym. Chem.* **2021**, *12*, 5704.

- [72] Y. Fujisawa, A. Asano, Y. Itoh, T. Aida, J. Am. Chem. Soc. 2021, 143, 15279.
- [73] Y. Yanagisawa, Y. Nan, K. Okuro, T. Aida, Science 2018, 359, 72.
- [74] J. Lin, Z. Peng, Y. Liu, F. Ruiz-Zepeda, R. Ye, E. L. G. Samuel, M. J. Yacaman, B. I. Yakobson, J. M. Tour, *Nat. Commun.* **2014**, *5*, 5714.